J Solid State Eletrochem (2004) 8: 82–88
DOI 10.1007/s10008-003-0358-z

ORIGINAL PAPER

Elvira Gómez · Albert Llorente · Xavier Alcobe
Elisa Vallés

Electrodeposition for obtaining homogeneous or heterogeneous cobalt-copper films

Received: 24 October 2002 / Accepted: 16 January 2003 / Published online: 23 September 2003

Abstract Direct electrodeposition of heterogeneous deposits may be an alternative method for preparing cobalt-copper coatings with magnetoresistive properties. Co-Cu electrodeposition was obtained in sulfate baths containing different citrate concentrations in order to prepare either homogeneous or heterogeneous Co-Cu deposits. X-ray diffraction (XRD) and voltammetric stripping analysis were used to study the kind of deposits formed. Citrate-free baths produced heterogeneous films, although dendritic growth was observed, thus increasing the deposit's thickness. Increasing the Cu(II)/Co(II) ratio in solution enabled the formation of smoother deposits. The presence of citrate at up to twice the total metallic concentration in the bath improved the morphological aspects of the deposits, their structural heterogeneity being maintained. Higher citrate concentrations induced the loss of heterogeneity, and both electrochemical and diffraction peaks tended towards single peaks. Homogeneous Co-Cu deposits, formed by a solid solution structure, were obtained in highly complexed citrate baths.

Keywords Cobalt-copper alloy films · Electrodeposition · X-ray diffraction

Introduction

In recent years, the preparation of magnetoresistive alloy thin films has been extensively studied in order to test their usefulness in sensor devices. The Co-Cu system is suitable for such a purpose because some heterogeneous Co-Cu alloys present high magnetoresistive values [1, 2, 3, 4, 5, 6, 7, 8, 9, 10] when cobalt particles of a defined size are dispersed in a copper matrix.

Heterogeneous Co-Cu films are usually prepared by physical methods such as sputtering [1, 2, 6, 11, 12], nebulized spray pyrolysis [13], electron beam evaporation [8, 9], rapid quenching [3, 14] or mechanical milling of the elements [15, 16]. A posterior annealing of the samples is usually performed in order to provide better separation of the cobalt granules from the copper matrix.

The electrodeposition technique has recently been used as an alternative method for preparing thin films of different alloys. However, despite the fact that the equilibrium phase diagram in the Co-Cu system allows negligible solubility of two metals at room temperature [17], electrodeposition has generally been found to produce a metastable solid solution when complexing agents are used for the simultaneous co-deposition of cobalt and copper. These homogeneous deposits require a posterior annealing of the samples in order to form cobalt precipitates in the matrix [4, 7, 18].

In previous electrodeposition studies [19, 20] we obtained homogeneous Co-Cu films of different composition that corresponded to solid solutions. The present study aimed to test whether electrodeposition could be used for the direct preparation of uniform, adequate heterogeneous Co-Cu alloys, without the need for posterior annealing of the samples. To this end, different solutions were tested, with and without complexing agents, in order to induce the electrodeposition of Co-Cu heterogeneous alloys.

Experimental

Solutions were prepared from $CuSO_4.5H_2O$, $CoSO_4.7H_2O$ and H_3BO_3, with a constant boric acid concentration of 30 g dm^{-3}. Different sodium citrate ($Na_3C_6H_5O_7.2H_2O$) concentrations between 0 and 1 mol dm^{-3} were used in order to control the

E. Gómez · A. Llorente · E. Vallés (✉)
Electrodep, Departament de Química Física,
Universitat de Barcelona, Martí i Franquès 1,
08028 Barcelona, Spain
E-mail: e.valles@qf.ub.es
Tel.: +34-93-4021234
Fax: +34-93-4021231

X. Alcobe
Serveis Cientificotècnics, Universitat de Barcelona,
Lluis Solé i Sabaris 1–3, 08028 Barcelona, Spain

simultaneous cobalt and copper co-deposition. All solutions were freshly prepared with water first doubly distilled and then treated with a Millipore Milli Q system. In all cases, the pH was adjusted to 3.5 by suitable addition of H_2SO_4. Before and during the experiments, solutions were de-aerated with argon. Deposition was performed at 20 °C.

Electrochemical experiments were carried out in a conventional three-electrode cell using an Autolab with PGSTAT30 equipment and GPES software. Working electrodes were vitreous carbon (Metrohm) and nickel rods (Johnson Matthey, 99.99%), both with an area of 0.0314 cm^2. The vitreous carbon electrode was polished to a mirror finish using alumina of different grades (3.75 and 1.87 μm) and cleaned ultrasonically for 2 min in water before each experiment. The nickel electrode was polished before each experiment using 4000 grade paper and diamond of different grades (6 and 1 μm), and then ultrasonically rinsed for 2 min in water. The counter electrode was a platinum spiral. The reference electrode was Ag|AgCl|NaCl (1 mol dm^{-3}) mounted in a Luggin capillary containing 0.5 mol dm^{-3} Na_2SO_4 solution. All potentials are referred to this electrode.

Voltammetric experiments were carried out at different scan rates between 5 and 50 mV s^{-1}, scanning at first to negative potentials. Only one cycle was run in each voltammetric experiment. Stripping analysis was always performed immediately after deposition, both in the deposition solution itself and in a blank solution (0.5 mol dm^{-3} Na_2SO_4). All deposits were obtained under stirring conditions ($\omega = 100$ rpm, magnetic stirrer).

The morphology of deposits was examined with a Hitachi S 2300 scanning electron microscope. Elemental composition was determined using an X-ray analyser incorporated into a Leica Cambridge Stereoscan S-360 (EDS).

X-ray diffraction (XRD) analysis was performed on a Philips MRD diffractometer in its parallel low-resolution optics. The Cu-K_α radiation ($\lambda = 1.5418$ Å) was selected by means of a diffracted-beam flat graphite monochromator crystal. Two experimental conditions were used. Diffractograms for the initial qualitative analysis were from $2\theta = 20$ to 100° with a step size of $2\theta = 0.05°$, a measuring time of 5 s per step and a beam size of 1×1 mm^2. $2\theta/\theta$ detailed scans were recorded for some samples in the range of the 311 reflection with a step size of $2\theta = 0.05°$, measuring times between 35 and 80 s per step and a beam size of 0.7×0.2 mm^2.

Results and discussion

Different sodium citrate concentrations were tested to obtain coherent and continuous heterogeneous Co-Cu deposits. For each solution, a voltammetric study was performed both on vitreous carbon and nickel electrodes in order to test the copper and cobalt co-deposition. Electrodeposition conditions were then selected to obtain Co-Cu coatings, whose morphology, composition and crystalline structure were analysed.

Citrate-free solutions

The Co-Cu electrodeposition from baths without complexing agent was analysed from two solutions containing different proportions of copper and cobalt sulfates. Owing to the different equilibrium potential of the Cu^{2+} and Co^{2+} reduction reactions in an uncomplexed state, copper(II) was always maintained as the minority ion, its deposition potential being clearly more favourable than that of cobalt.

For the first solution studied, that containing 0.01 mol dm^{-3} of Cu(II) and 2 mol dm^{-3} of Co(II), the voltammetric response under stationary conditions showed a clearly separate reduction process (Fig. 1A and B): a first copper reduction peak, centred around −150 mV (magnified in Fig. 1B), followed by a new reduction current related to the start of cobalt deposition was observed. The copper reduction peak (Fig. 1B) showed the typical shape of a diffusion-controlled process. When low cathodic limits were used, only one oxidation peak was detected, corresponding to copper oxidation. Decreasing the cathodic limit, a new oxidation peak was observed in the anodic scan, prior to copper oxidation. As the position of the copper oxidation peak was constant for different cathodic limits, it can be deduced that the reduction current in excess of the diffusion-limited current for copper deposition, detected from around −800 mV, was due to cobalt deposition. Similarly, the more negative oxidation peak can be assigned to the oxidation of the deposited cobalt.

Potentiostatic transients over the vitreous carbon electrode confirmed the behaviour demonstrated by the voltammetric results. At low deposition potentials, only copper deposition was observed (Fig. 2, curve a). Decreasing deposition potentials to sufficiently negative values produced a first peak in the j vs. t transient, followed by a second growth in the curve (Fig. 2, curves b

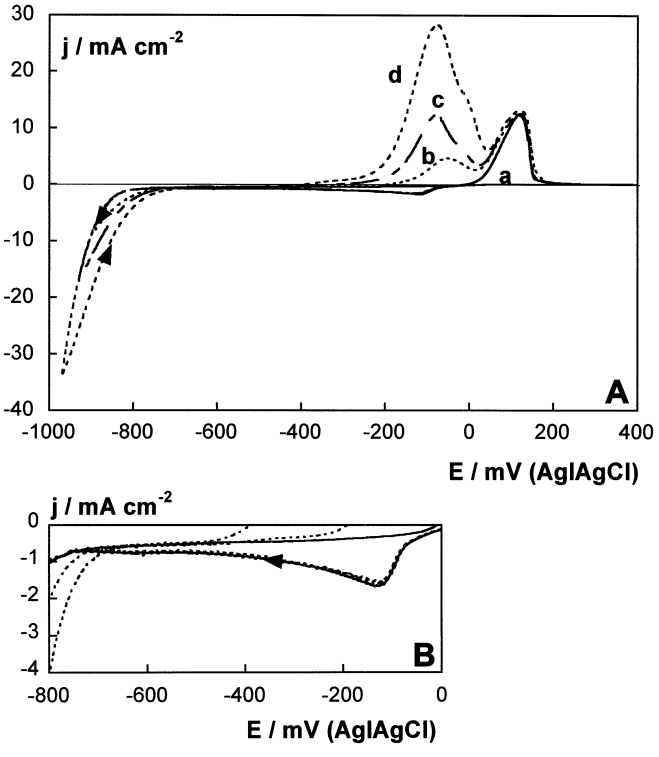

Fig. 1 **A** Cyclic voltammograms of a 2 mol dm^{-3} $CoSO_4$ + 0.01 mol dm^{-3} $CuSO_4$ + 30 g dm^{-3} H_3BO_3 solution; 50 mV s^{-1}; vitreous carbon electrode. Starting potential: 100 mV. Cathodic limit: *a* −800, *b* −900, *c* −930 and *d* −970 mV. **B** Magnified detail of **A** in the potential range of 0 to −800 mV

and c), revealing that cobalt deposition took place over the previous copper deposited.

Under quiescent conditions, galvanostatic transients at different current densities showed a clear change with respect to time. The potential first evolved to a value corresponding to copper deposition, and then reached a value at which cobalt deposition was possible. Only when copper(II) was depleted around the electrode did cobalt(II) start to deposit and the recorded potential corresponded to cobalt deposition. Under stirred conditions it was only possible to attain a stationary potential when the total applied current was lower than the diffusion-limited current for copper deposition.

The voltammetric stripping response of the deposits obtained under moderate stirring conditions always showed two separate oxidation peaks when sufficiently negative potentials were applied (Fig. 3). The relative height of these two oxidation peaks depended on the deposition potential. The same stripping profiles were observed using the deposition solution or a blank solution (0.5 mol dm^{-3} Na_2SO_4). When the current efficiency was close to 100%, the relative heights of the two peaks indicated the relative presence of cobalt and copper in the films, the first oxidation peak corresponding to cobalt oxidation and the more positive to copper oxidation.

Thicker deposits were obtained over nickel electrodes, as this metallic substrate favours their adherence. The dependence of film composition on agitation meant that uniform stirring over the substrate was required. Final deposits obtained from this solution were not very homogeneous in morphology, and became more dendritic with decreasing deposition potentials and increasing deposition time. Only low charges (< 1.5 C cm^{-2}), leading to thicknesses lower than 0.6 μm, produced relatively uniform final deposits (Fig. 4A). Structural analysis of the coatings obtained at similar conditions but greater deposition charge revealed that the films were clearly heterogeneous, the diffractograms showing peaks corresponding to the face centred cubic (f.c.c.) copper and the f.c.c. cobalt structures (Fig. 4B).

Increasing the Cu(II)/Co(II) solution ratio, some differences were observed in both electrochemical and morphological results. For a solution containing

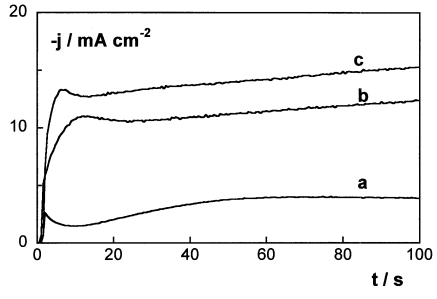

Fig. 2 Potentiostatic transients of the same solution and electrode as in Fig. 1 at *a* −800, *b* −875 and *c* −900 mV

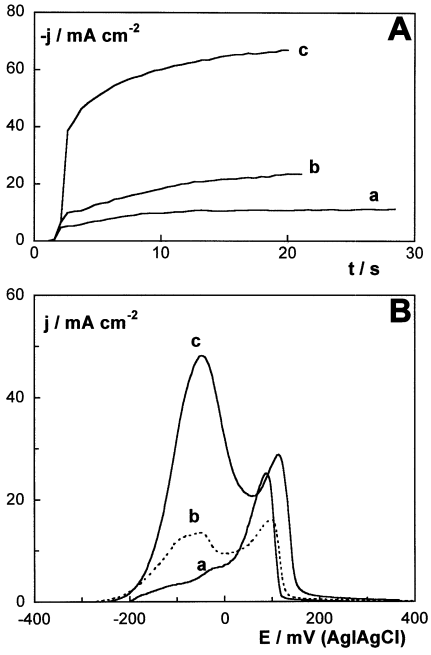

Fig. 3 **A** Potentiostatic transients, obtained at $\omega = 100$ rpm, of the same solution and electrode as in Fig. 1 at *a* −850, *b* −900 and *c* −950 mV. **B** Potentiodynamic stripping curves at 10 mV s^{-1} corresponding to deposits obtained from the *j* vs. *t* transients of **A**

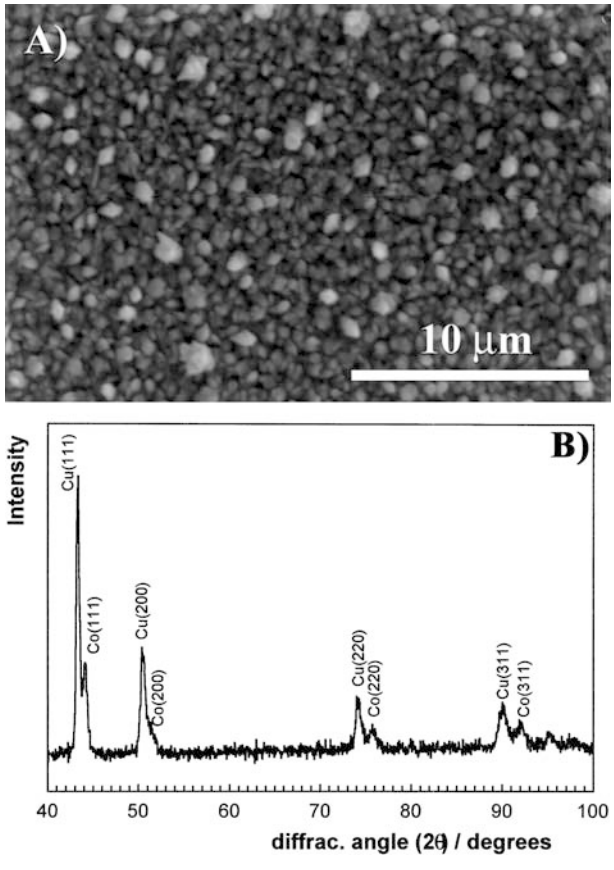

Fig. 4 **A** SEM micrographs of a deposit obtained at −950 mV for 20 s from the solution of Fig. 1. Nickel electrode; $\omega = 100$ rpm; 50% Co; thickness: 0.43 μm. **B** X-ray diffractogram of the deposit obtained under the same conditions as in **A**, but for 1200 s

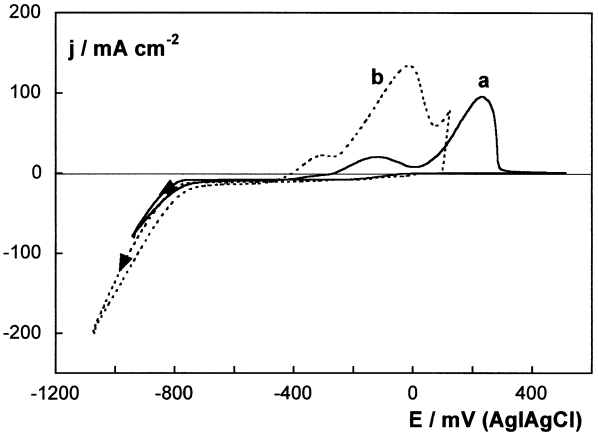

Fig. 5 Cyclic voltammograms of a 0.9 mol dm^{-3} $CoSO_4 + 0.1$ - mol dm^{-3} $CuSO_4 + 30$ g dm^{-3} H_3BO_3 solution; 5 mV s^{-1}. *a* Vitreous carbon electrode; *b* nickel electrode

0.1 mol dm^{-3} of Cu(II) and 0.9 mol dm^{-3} of Co(II), and using similar scan rates as for the 0.01 mol dm^{-3} Cu(II)/ 2 mol dm^{-3} Co(II) solution, the voltammetric response showed a lower separation of the oxidation peaks. However, decreasing to 5 mV s^{-1} also produced a clear separation of peaks for both vitreous carbon and nickel electrodes (Fig. 5). As the copper(II) concentration was increased with respect to the first solution, there was a simultaneous increase in copper deposition in the cobalt reduction zone. However, the position of the two oxidation maxima was not dependent on the cathodic limit used in the voltammetric scan, revealing that although copper and cobalt may co-deposit in a defined potential zone, a heterogeneous copper + cobalt deposit was in fact formed.

The deposits obtained from this solution at low deposition charges (< 5 C cm^{-2}) consisted of polyhedral crystals of varying size (Fig. 6A) which showed a similar morphology to that observed for a higher [Co(II)]/ [Cu(II)] ratio. X-ray diffractograms showed that heterogeneous deposits, formed by a mixture of cobalt and copper, were also obtained from this solution. The cobalt percentage in these thin deposits increased when either the deposition potential or the current densities were made more negative. In contrast, increasing the level of agitation of the solution during deposition led to a decrease in the cobalt percentage, because the process of copper deposition is controlled by diffusion.

Increasing the deposition charge, it was observed that non-uniformity in the deposits and copper-rich dendrites was observed over the first deposit (Fig. 6B).

Sodium citrate additions

A range of sodium citrate concentrations were added to the 0.1 mol dm^{-3} Cu(II)/0.9 mol dm^{-3} Co(II) solution in order to favour the formation of more homogeneous and less dendritic deposits. Citrate concentration values between 0.1 and 1 mol dm^{-3} were tested.

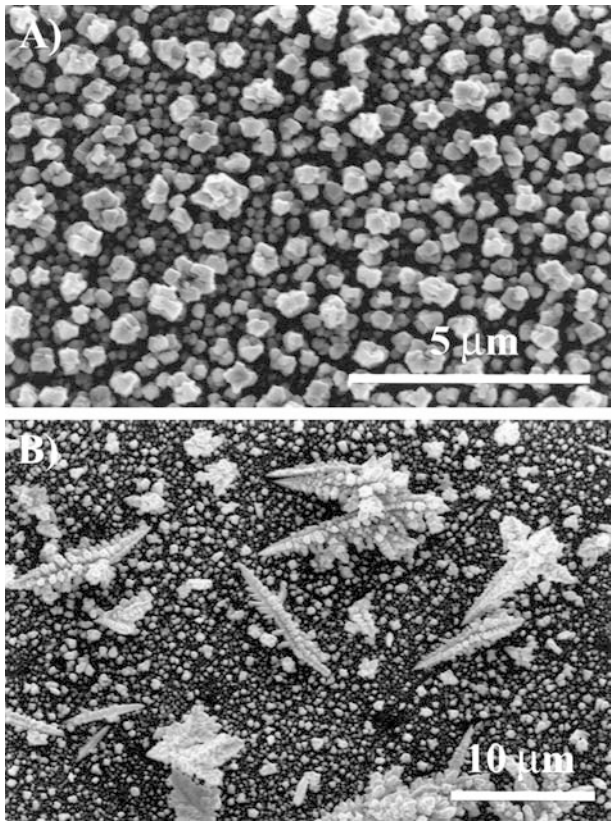

Fig. 6 SEM micrographs of the deposits obtained from the solution of Fig. 5 at −1100 mV; nickel electrode; $\omega = 100$ rpm. **A** 50 s, 35% Co, thickness 0.85 µm; **B** 300 s

Voltammetric experiments over the vitreous carbon electrode showed that an increase in citrate concentration approached the potentials at which the two metals were deposited (Fig. 7). Copper reduction was clearly shifted (Fig. 7B) towards more negative potentials, revealing an important copper complexation, whereas the start of cobalt co-deposition was less modified for the different citrate concentrations used. The corresponding oxidation response tended toward a single oxidation peak when the citrate concentration was gradually increased (Fig. 7A), demonstrating that such increases produce gradual changes in the deposition process.

For the highest citrate concentrations studied ([citrate] > 0.5 mol dm^{-3}), voltammetric and stripping results showed that only one oxidation peak was ever obtained for the different cathodic limits applied. The position of this peak clearly moved towards the position of the pure cobalt oxidation peak as the cathodic limit was gradually decreased (Fig. 8), this corresponding to the formation of a Co-Cu solid solution [19, 20]. These results confirm that deposition through citrate complexes favours the simultaneous co-deposition of cobalt and copper and induces a homogeneous alloy.

The deposits obtained, both potentiostatically and galvanostatically, from each of the analysed solutions

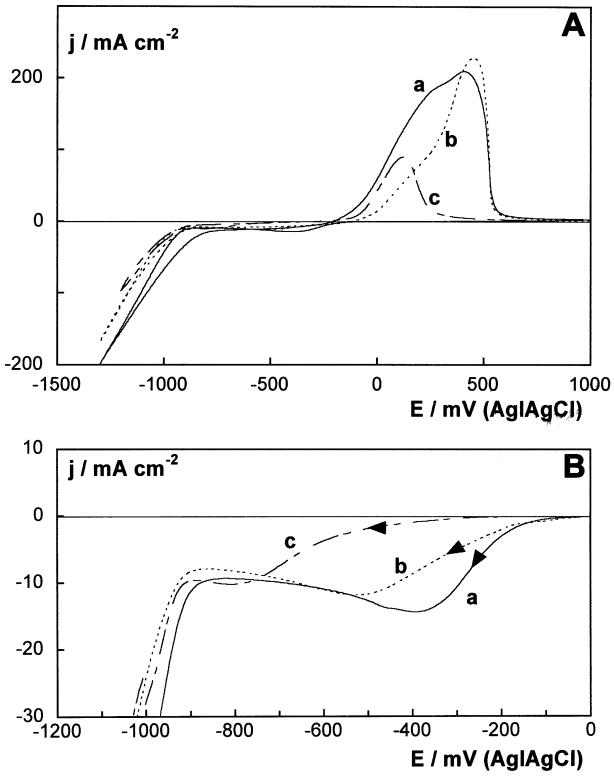

Fig. 7 **A** Cyclic voltammograms at 50 mV s^{-1} on vitreous carbon electrode; 0.9 mol dm^{-3} $CoSO_4$ + 0.1 mol dm^{-3} $CuSO_4$ + 30 g dm^{-3} H_3BO_3 + *a* 0, *b* 0.1 and *c* 1 mol dm^{-3} $Na_3C_6H_5O_7$ solution. **B** Detailed zone of the copper reduction peak

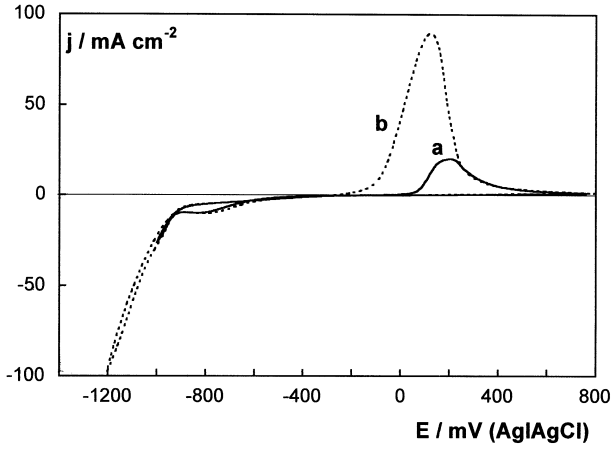

Fig. 8 Cyclic voltammograms of a 0.9 mol dm^{-3} $CoSO_4$0.1 mol dm^{-3} $CuSO_4$ + 30 g dm^{-3} H_3BO_3 + 1 mol dm^{-3} $Na_3C_6H_5O_7$ solution; 50 mV s^{-1}; vitreous carbon electrode. Cathodic limit: *a* −1000 and *b* −1200 mV

were compared. From the 0.1 mol dm^{-3} citrate solution it was possible to obtain non-dendritic layers at deposition charges lower than 15 C cm^{-2}. The solutions containing low citrate concentrations produced rough deposits (Fig. 9A), whereas increasing the citrate concentration led to more homogeneous and flat deposits

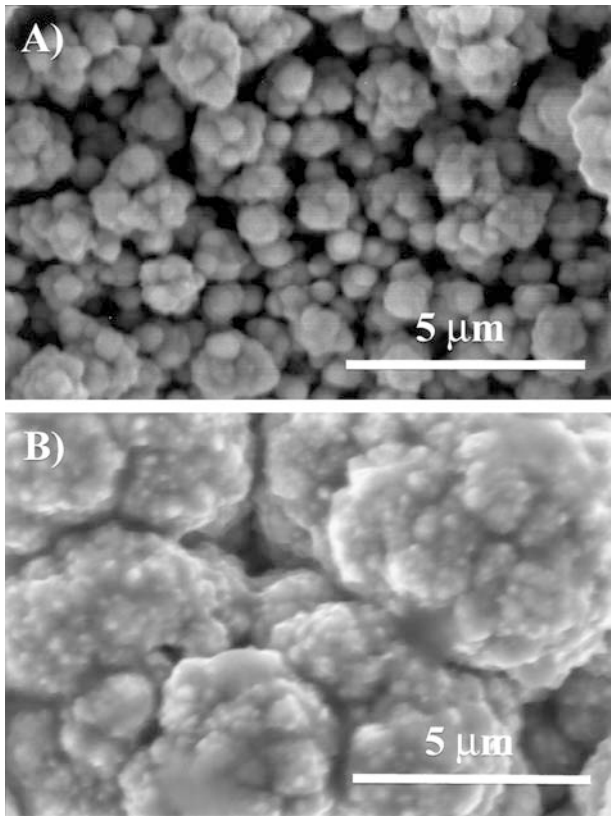

Fig. 9 **A** SEM micrographs of a deposit obtained from a 0.9 mol dm^{-3} $CoSO_4$ + 0.1 mol dm^{-3} $CuSO_4$ + 30 g dm^{-3} H_3BO_3 + 0.1 mol dm^{-3} $Na_3C_6H_5O_7$ solution; nickel electrode; $\omega = 100$ rpm; −950 mV for 1000 s; 37% Co. **B** SEM micrographs of a deposit obtained from a 0.9 mol dm^{-3} $CoSO_4$ + 0.1 mol dm^{-3} $CuSO_4$ + 30 g dm^{-3} H_3BO_3 + 1 mol dm^{-3} $Na_3C_6H_5O_7$ solution; nickel electrode; $\omega = 100$ rpm; −1000 mV for 2000 s; 50% Co

(Fig. 9B). The deposits became dendritic in citrate-free solutions, whereas non-dendritic homogenous deposits were produced by increasing the citrate concentration. The addition of citrate to solutions led to more uniform deposits being obtained, even for thick coatings.

In order to investigate the influence of the bath's citrate content on the heterogeneity of the deposits, and to follow the gradual structural changes of these deposits, XRD analyses of the deposits obtained at the same deposition charge from different citrate concentration solutions were performed. Low deposition charges were used to avoid the formation of dendritic copper structures in the case of the citrate-free solution. In all cases, the signal corresponding to vitreous carbon was found to be superimposed onto the signal of the Co-Cu layer. The evolution of the samples' diffraction peak positions and intensities was also analysed and detailed scans of the 311 reflections were obtained. This peak, obtained at high θ values, was chosen because it showed the greatest separation between copper and cobalt positions. Moreover, no substrate peaks (of vitreous carbon) were detected in this 2θ range.

Peak profile analysis was performed using pseudo-Voight functions. The 2θ intensities and the full width at

Table 1 Influence of citrate concentration and deposition potential on the positions and relative intensities of the 311 diffraction peaks. EDS-determined metal content

[Citrate]/ (mol dm^{-3})	E (mV)	Co (%)	2θ (Cu)	% Intensity (Cu)	2θ (Co)	% Intensity (Co)	FWHM
–	−1000	32–63	90.37	40	91.91	60	1.29
–	−1100	40–80	90.68	24	92.08	76	1.13
0.1	−1000	30–56	90.85	54	91.59	46	1.06
0.1	−1100	37–42	90.37	19	91.58	81	1.20
0.2	−1000	55	91.35				1.24
0.2	−1100	72	91.65				1.28
0.8	−1000	50	91.05				1.23

half maximum (FWHM) were refined for every observed peak. Table 1 lists the 2θ positions, the relative intensities of the Cu and Co peaks when both were observed, and the FWHM of the adjusted peaks. When double peaks were observed, the FWHM of both peaks were settled as equal values. The table shows that non-uniform composition is detected for the samples obtained from solutions containing citrate concentrations lower than 0.2 mol dm^{-3}.

For deposits obtained from the citrate-free solution, two separate peaks were clearly observed, as with those obtained for different Co(II) and Cu(II) concentrations and thicker deposits (Fig. 4B). The obtained positions are close to those known to exist for Cu and Co fcc structures (89.93 for Cu and 92.23 for Co). Decreasing the deposition potential, an increase in the relative intensity of the Co peak is observed, indicating an increased cobalt percentage in the deposit.

All results indicated that increasing the citrate concentration in the baths enabled the evolution from double to single peaks to be observed. A concentration of 0.1 mol dm^{-3} revealed double peaks indicative of heterogeneous films, whereas at concentrations of 0.2 and 0.8 mol dm^{-3} single peaks were observed, indicative of solid solution formation. Similarly, the relative intensity of the Co peak increases upon decreasing the deposition potential in the 0.1 mol dm^{-3} baths. When solid solutions are formed, the position of the peak seems closer to the known Co position when the overall Co composition is higher.

Conclusions

Electrodeposition was shown to be a useful tool for preparing either homogeneous or heterogeneous deposits, depending on solution composition and electrodeposition conditions.

Electrodeposition from electrolytes containing Co(II) and Cu(II) ions in an uncomplexed or weakly complexed enabled heterogeneous Co-Cu deposits to be prepared, in which copper and cobalt deposited separately. However, these deposits were uniform and coherent at low deposition charges. When thicker deposits were prepared, even under stirring conditions they developed a dendritic morphology, due to the fast and favoured deposition of copper over the initial Co-Cu deposit. Voltammetric and stripping curves provided an estimate of the cobalt/copper ratio present in the prepared thin films.

When sodium citrate was used at concentrations higher than 0.2 mol dm^{-3}, the important complexation of ions, especially that of copper(II), slows copper deposition and favours simultaneous copper and cobalt co-deposition. These solutions, regardless of the thickness, produced homogeneous and uniform deposits that correspond to a solid solution. The position of the peaks in X-ray diffractograms and voltammetric and stripping curves provide estimates of the cobalt percentage in the deposits.

Citrate concentrations around 0.1 mol dm^{-3} proved adequate for preparing granular heterogeneous Co-Cu coatings. However, this amount of sodium citrate in solution is not enough to complex all copper ions, as the manner that deposition occurs simultaneously from free and complexed ions. Although non-flat deposits were obtained in these conditions, sufficiently coherent and uniform deposits were prepared for coatings of a few microns.

Acknowledgements The authors wish to thank the Serveis Cientificotècnics (Universitat de Barcelona) for providing equipment. This research was supported financially by contracts MAT 2000-0986 from the Spanish Comisión Interministerial de Ciencia y Tecnología (CICYT) and by the Comissionat of the Generalitat de Catalunya under Research Project SGR 2000-017.

References

1. Berkowitz AE, Mitchell JR, Carey MJ, Young AP, Zhang S, Spada FE, Parker FT, Huttem A, Thomas G (1992) Phys Rev Lett 68:3745
2. Xiao JQ, Jiang JS, Chien CL (1992) Phys Rev Lett 68:3749
3. Setna RP, Cerezo A, Hyde JM, Smith GDW (1994) Appl Surf Sci 76/77:203
4. Fedosyuk VM, Kasyutich OI, Ravinder D, Blythe HJ (1996) J Magn Magn Mater 156:345
5. Schwarzacher W, Lashmore DS (1996) IEEE Trans Magn 32:3133
6. Tsunoda M, Okuyama K, Ooba M, Takahashi M (1998) J Appl Phys 83:7004
7. Zaman H, Yamada A, Fukuda H, Ueda Y (1998) J Electrochem Soc 145:565
8. Viegas ADC, Geshev J, Schmidt JE, Ferrari EF (1998) J Appl Phys 83:565

9. Kakazei GN, Krovetz AF, Lesnik NA, Pereira de Azevedo MM, Pogorelov YuG, Bondorkova GV, Silantiev VL, Sousa JB (1999) J Magn Magn Mater 196:29
10. Ueda Y, Houga T, Zaman H, Yamada A (1999) J Solid State Chem 147:274
11. Childress JR, Chien CL (1991) Phys Rev B 43:8089
12. Childress JR, Chien CL (1991) J Appl Phys 70:5885
13. Parashar S, Raju AR, Rao CNR (1999) Mater Chem Phys 61:46
14. Schmool D, Garcia-Arribas A, Abad E, Garitaonandia JS, Fdez-Gubieda ML, Barandiaran JM (1999) J Magn Magn Mater 203:73
15. Dellogu F, Pintore M, Enzo S, Cardellini F, Contini V, Montone A, Rosato V (1997) Philos Mag B 76:651
16. Liu BX, Ma E, Li J, Huang LJ (1997) Nucl Instr Methods Phys Res B 19/20:682
17. ASM (1992) Alloy phase diagrams. In: Baker H (ed) ASM handbook, vol.3. ASM International, Ohio
18. Blythe HJ, Fedosyuk VM (1996) J Magn Magn Mater 155:352
19. Gómez E, Llorente A, Vallés E (2000) J Electroanal Chem 495:19
20. Gómez E, Labarta A, Llorente A, Vallés E (2001) J Electroanal Chem 517:63